frontiers in Chemistry

ORIGINAL RESEARCH
published: 15 July 2021
doi: 10.3389/fchem.2021.678993

A Multifunctional 3D Supermolecular Co Coordination Polymer With Potential for CO_2 Adsorption, Antibacterial Activity, and Selective Sensing of Fe^{3+}/Cr^{3+} Ions and TNP

Xiaojing Zhou, Lili Liu, Hang Kou, Shimei Zheng, Mingjun Song, Jitao Lu and Xishi Tai**

School of Chemical and Chemical Engineering and Environmental Engineering, Weifang University, Weifang, China

A 3D supermolecular structure $[Co_3(L)_2$ (2,2′-bipy)$_2](DMF)_3(H_2O)_3$ 1) (H_3L = 4,4′,4″-nitrilotribenzoic acid) has been constructed based on H_3L, and 2,2′-bipy ligands under solvothermal conditions. Compound **1** can be described as a (3, 6)-connected kgd topology with a Schläfli symbol $(4^3)_2(4^6.6^6.8^3)$ formed by $[Co_3(CO_2)_6]$ secondary building units. The adsorption properties of the activated sample 1a has been studied; the result shows that 1a has a high adsorption ability: the CO_2 uptakes were 74 $cm^3 \cdot g^{-1}$ at 273 K, 50 $cm^3 \cdot g^{-1}$ at 298 K, the isosteric heat of adsorption (Q_{st}) is 25.5 kJ mol^{-1} at zero loading, and the N_2 adsorption at 77 K, 1 bar is 307 cm^3 g^{-1}. Magnetic measurements showed the existence of an antiferromagnetic exchange interaction in compound **1**, besides compound **1** exhibits effective luminescent performance for Fe^{3+}/Cr^{3+} and TNP.

Keywords: sensing, Fe^{3+}/Cr^{3+}, TNP, antibacterial, CO_2 adsorption, magnetism, coordination polymer

OPEN ACCESS

Edited by:
Isurika R. Fernando, University of Sri Jayewardenepura, Sri Lanka

Reviewed by:
Tangxin Xiao, Changzhou University, China
Ji-Yong Zou, Jiangxi Academy of Sciences, China
Manoj Trivedi, University of Delhi, India

****Correspondence:***
Jitao Lu
lujitao@foxmail.com
Xishi Tai
taixs@wfu.edu.cn

Specialty section:
This article was submitted to Supramolecular Chemistry, a section of the journal Frontiers in Chemistry

Received: *10 March 2021*
Accepted: *07 June 2021*
Published: *15 July 2021*

Citation:
Zhou X, Liu L, Kou H, Zheng S, Song M, Lu J and Tai X (2021) A Multifunctional 3D Supermolecular Co Coordination Polymer With Potential for CO_2 Adsorption, Antibacterial Activity, and Selective Sensing of Fe^{3+}/Cr^{3+} Ions and TNP. Front. Chem. 9:678993. doi: 10.3389/fchem.2021.678993

INTRODUCTION

Nowadays, the rapid detection of toxic organic and heavy metal ion pollutants has attracted more and more attention due to their harmful effects on the environment and human life (Rasheed and Nabeel, 2019; Haldar et al., 2020). For instance, nitroaromatic explosives (NACs), which include nitrobenzene, 2,4,6-trinitrophenol (TNP), 2-nitrotoluene, 2,4-dinitrotoluene, nitrobenzene, 4-nitrotoluene and 3-nitrotoluene, have many application in the chemical industry and can cause terrorism and environmental issues. Among NACs, TNP is highly toxic, it harms the microorganisms and the human body (Wollin and Dieter, 2005). Likewise, heavy metal pollutants are not degradable and tend to accumulate in ecosystems, imposing a threat to human beings because of their toxicity and carcinogenicity (Jia et al., 2017; Peng et al., 2018; Ashraf et al., 2019; Cai et al., 2019). Fe^{3+} is an abundant and essential transition metal for biological organisms, and plays an important role in biological processes, such as enzymatic reactions, nitrogen fixation in nitrogenases, and oxygen transport. It is also well known that inadequate or excess iron concentration can induce serious health problems including anemia, Alzheimer's disease, liver and kidney damage, diabetes and heart disease, mitochondrial DNA damage (Harigae, 2018; VanderMeulen and Sholzberg, 2018; Wallace et al., 2018; Sahoo and Crisponi, 2019; Fan et al., 2020). Similarly, Cr^{3+} has mutagenicity and cytogenetic toxicity, the scarcity or excess uptake of Cr^{3+} results in cardiovascular diseases and diabetes, mutations or malignant cells (Paul et al., 2015; Zhang et al., 2015; Dong et al., 2016; Rasheed and Nabeel, 2019), so it is urgent and necessary to detect metal ion pollutants in solution for the human security and environmental protection.

Various techniques have been developed to detect Fe^{3+}/Cr^{3+} and TNP (Chen et al., 2018; Pavlačka et al., 2016; Sadak et al., 2017; Tian et al., 2017; Goswami et al., 2013; Wen et al., 2002); among them, fluorescence analysis has been very popular due to its simplicity, sensitivity, fast response, economical way, low interference (Carter et al., 2014; Guo et al., 2014). Therefore the development of excellent fluorescence sensors for the sensitivity of Fe^{3+}/Cr^{3+} and TNP has become a focus. The use of coordination polymers for fluorescence analysis has been explored extensively (Zhang et al., 2018; Hu et al., 2014; Yi et al., 2016). The coordination polymers, built up from organic ligands and metal ions or clusters, are porous materials suitable for various applications including luminescence, magnetism, gas adsorption and separation, as well as catalysis, drug delivery, and proton conduction (Kurmoo, 2009; Huxford et al., 2010; Sun et al., 2013; Yamada et al., 2013; Li et al., 2014; Liu et al., 2014; Zhou. and Kitagawa, 2014; Chughtai et al., 2015; Lustig et al., 2017; Espallargas and Coronado, 2018).

Over the past few years, many luminescent coordiantion polymers have been synthesized to detect metal ions, anions, pH value, small molecules, gases and vapors (Kurmoo, 2009; Lan et al., 2009; Li et al., 2013; Ma et al., 2013; Zhang et al., 2015; Yu et al., 2017; Mi et al., 2019; Tang et al., 2020), in this contribution, we select a tricarboxytriphenylamine (H_3L) as a ligand to construct a new Co coordiantion polymer is mainly based on the following considerations: 1) The conjugated and photoactive triphenylamine moiety makes the MOFs highly fluorogenic; 2) Lewis base N sites on the internal surface of the framework can improve the sensing of ions and adsorption of CO_2; 3) The carboxylate groups have multiple coordination modes to coordinate the metal ions, and the uncoordinated O atoms can provide interaction sites for the metal ions and NACs (specifically, TNP containing three NO_2 groups). Meanwhile, among the MOF sensors, highly economical and abundant Co. ions with magnetic properties have rarely been studied as sensors, mainly because the non-d^{10} electronic structures have low emission performance owing to d–d transitions (Mishra et al., 2014; Chen et al., 2017; Zhang et al., 2018; Zhao et al., 2018).

For the recent years, significant progress has been expended on the development of materials for CO_2 capture, because CO_2 is responsible for the global warming. Utilizing the activated carbon, zeolites or amine solutions for absorbing CO_2 are considered the most adequate adsorbents, though the insufficient uptake capacity and high expense prevent these materials mass production (Zhang et al., 2014).

Many human diseases and infections are caused by unsafe drinking water and food containing bacteria such as *Escherichia coli*, *Staphylococcus aureus.* As to the low molecular weight antibacterial materials, they have many disadvantages, such as toxicity to the environment, short-term antibacterial activity. Hence, there is an urgent need for the development of effective antibacterial materials (Haendel et al., 2014; Kaur et al., 2020; Saira et al., 2020).

Taking the luminescence properties, CO_2 adsorption and antibacterial activity into consideration, we used the coordination polymer as the multifunctional material for sensitivity as well as CO_2 adsorption and antibacterial activity.

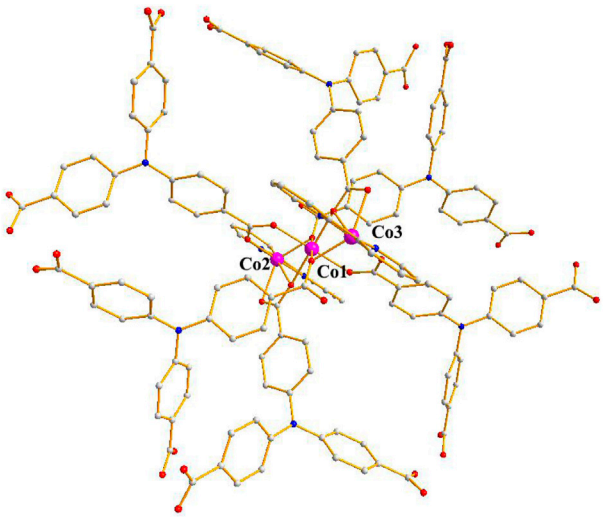

FIGURE 1 | The coordination mode of Co atoms in compound **1** (C: Gray, N: Blue, Co:Purple, O: Red).

In the manuscript, we obtained a Co. based coordiantion polymer $[Co_3(L)_2\ (2,2'\text{-bipy})_2](DMF)_3(H_2O)_3$ (denoted as compound **1**) under solvothermal conditions which has been utilized as a multifunctional MOF with preferential CO_2 adsorption, antibacterial activity, selective sensing of metal ions (Fe^{3+}, Cr^{3+}) and TNP, meanwhile, magnetic measurements show that there exists an antiferromagnetic exchange interaction in compound **1**.

MATERIALS AND METHODS

Synthesis of Compound 1

$Co.(NO_3)_2{\bullet}6H_2O$ (29.1 mg), H_3L (18.8 mg), and 2,2′-bipy (15.6 mg), *N*,*N*-dimethylformamide (3 ml), distilled water (1 ml), and ethanol (1 ml) were mixed in a 15 ml Teflon-lined stainless steel autoclave and heated at 100 °C for 72 h. Upon cooling at room temperature, purple crystals were prepared, which were washed with DMF and dried at 60°C for 6 h. Yield 38% (based on H_3L), IR (KBr 4000–400 cm^{-1}) 3463 (w), 3082 (w), 2,793 (w), 2,496 (w), 1,593 (s), 1,388 (s), 1,191 (w), 1,036 (w), 803 (m), 768 (m), 704 (m), 636 (w), 485 (m). Elemental analysis (%): Calcd for: $C_{71}H_{67}Co_3N_9O_{18}$: C 56.39, H 4.43, N 8.34; Found: C 56.41, H 4.29, N 8.37.

RESULTS AND DISCUSSION

Crystal Structure of Compound 1

The single-crystal X-ray data were collected using the X-ray diffraction technique and the results showed that crystallization of compound 1 in the monoclinic space group *C*2/*c* and the presence of two independent Co. atoms, one 2,2′-bipy molecule, and one linker (L^{3-}) in the asymmetric unit of 1 (**Supplementary Figure S1**). The Co1 atom is involved in

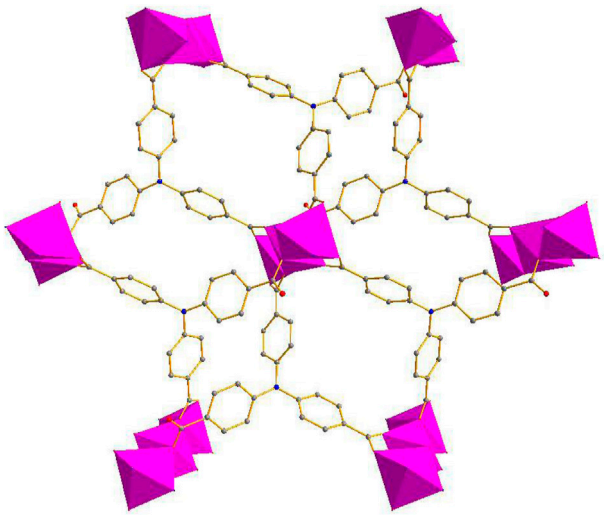

FIGURE 2 | The 2D framework of compound **1** (Co:Purple, O: Red, N: Blue, C: Gray).

coordination with six O atoms of the carboxylates of 6 L^{3-} ligands, showing an octahedral configuration (Co–O = 2.053–2.108 Å), the six-coordinated Co2 or its symmetry-related Co3 atom displays a distorted octahedral configuration, which is bonded with four carboxylate O atoms from 3 L^{3-} ligands, and 2 N atoms from one 2,2′-bipy molecule, Co2–O and Co2–N or Co3–O and Co3–N are in the range of 2.007–2.183 Å and 2.085–2.115 Å, respectively (**Figure 1**) (Mistri et al., 2017; Zhou et al., 2019), the bonding mode of the carboxylate toward the six Co^{2+} ions is μ^6-η^1:η^2:η^1:η^1:η^2:η^0 (**Supplementary Scheme 1** in the Supplementary Information), the adjacent Co1–Co3 atoms (Co···Co. separation, 3.168–6.337 Å) are united together by six carboxylates to form trinuclear Co.(II) clusters, each cluster can be connected to the adjacent ones to evolve a unique bylayer 2D framework, which contains quadrangle grids with a size of 7.0 Å × 6.4 Å running along the b-axis (atom-to-atom distance) (**Figure 2**). The 2D layers are then further converted into a 3D (supramolecular) structure via interactions of π–π stacking with the distance of 3.317 Å (**Figure 3**). The solvent-accessible volume in compound 1 was found to be 28.8 % (calculated using the PLATON software.12 after removal of solvent molecules).

If the L^{3-} ligands are defined as three-connected nodes, and the trinuclear Co.(II) cluster as six-connected nodes, the entire structure of Co. coordiantion polymer can be denoted as a (3, 6)-connected two-nodal net with a point symbol of $\{4^3\}_2\{4^6.6^6.8^3\}$, displaying the kgd topology (**Supplementary Figure S2**) (Kim et al., 2012; Wang et al., 2014).

Gas Sorption Experiment

The as-synthesized compound **1** was subjected to stirring with methanol at ambient temperature for 24 h to remove the solvent in the pores, followed by filtration of the compound and keeping at 60°C for 6 h in an oven. The compound was then heated for 24 h at 100°C under a vacuum to obtain the activated sample, 1a. The N_2 adsorption isotherm was acquired at 77 K, the result indicates that 1a displays a reversible type-I adsorption isotherm with the Brunauer–Emmett–Teller (BET) surface area of 658 $m^2 \cdot g^{-1}$, and the N_2 uptake (1 atm) reached 307 $cm^3 \cdot g^{-1}$ (**Figure 4A**). Meanwhile, the CO_2 adsorption isotherms for 1a were measured at 273 and 298 K; at 273 K (1 atm), and 298 K (1 atm) the CO_2 uptakes reached a maximum of 74 $cm^3 \cdot g^{-1}$ and 50 $cm^3 \cdot g^{-1}$, respectively (**Figure 4B**). The PXRD pattern of compound 1a remained stable after the adsorption of N_2 and CO_2 (**Supplementary Figure S11**). Considering the adsorption isotherm at 298 K, the observed CO_2 adsorption capacity of 1a is better than the metal-organic frameworks including

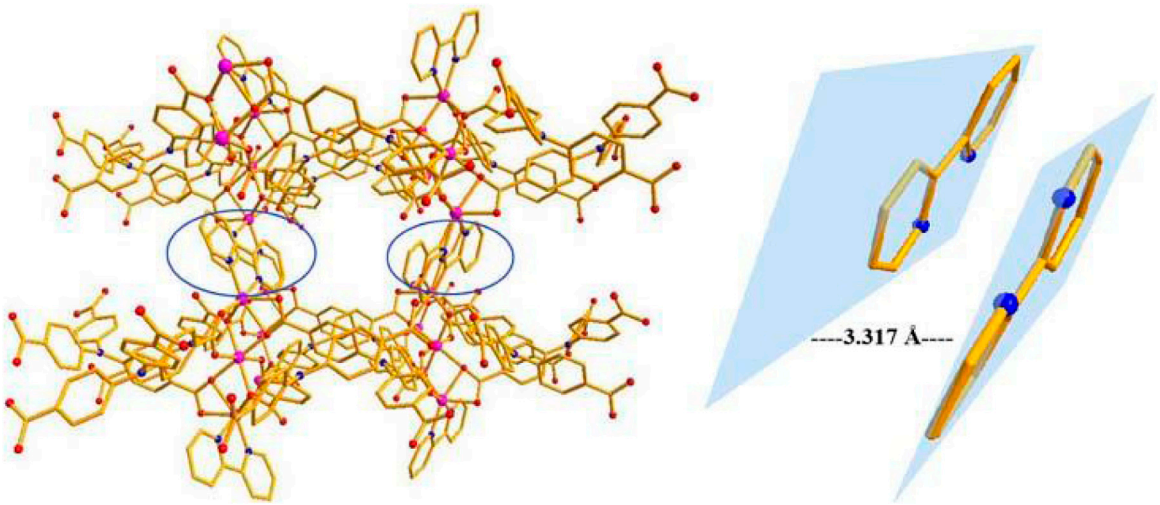

FIGURE 3 | The structure of compound **1** and interactions of π–π stacking (C: Gray, O: Red, N: Blue, Co:Purple).

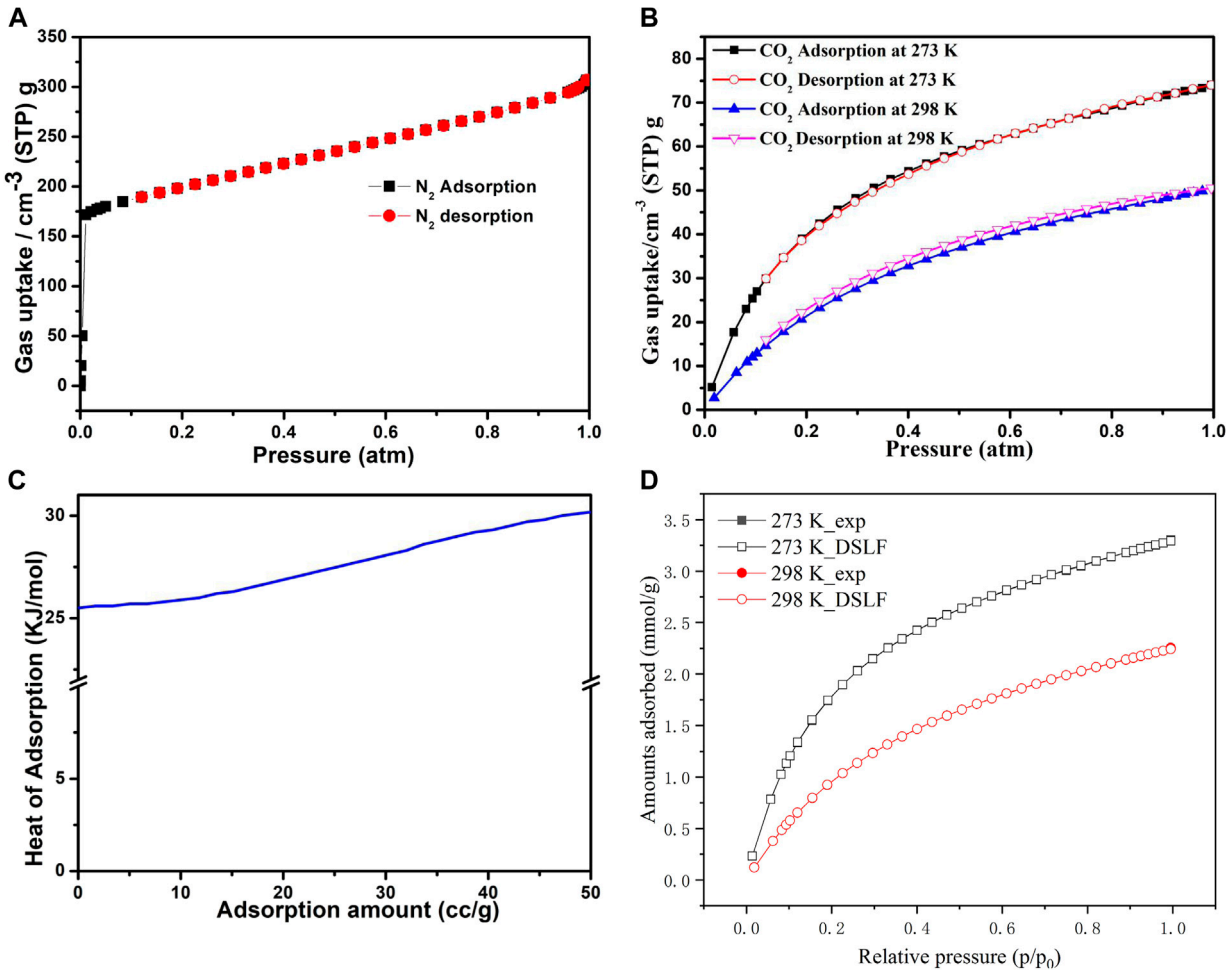

FIGURE 4 | (A) N_2 adsorption isotherms of 1a at 77 K; **(B)** CO_2 adsorption isotherms of **1a** at 273 K, 298 K; **(C)** Heat of CO_2 adsorption as a function of uptake amount; **(D)** The DSLF model for CO_2 adsorption isotherms.

$[Zn(BPTC)_{0.5}\ (Tz)]\bullet DMF\bullet CH_3OH$, JUC-MOF56, $\{[Cd_2\ (tdz)_2\ (4,4'\text{-bpy})_2]\bullet 6.5H_2O\}n$, $[Zn_2\ (TCA)\ (BIB)_{2.5}]\bullet(NO_3)$, $([Zr_6O_4(OH)_8(H_2O)_4(BTEB)_2]$, and $\{[Cd_4\ (hbhdpy)_2\ (bdc\text{-}NH_2)_3\ (DMA)_2]\bullet(H_2O)_4\}n$ that are summarized in **Supplementary Table S3** (Hong et al., 2017; Kong et al., 2018; Yao et al., 2018; Zhou et al., 2018; Liu et al., 2019). The adsorption isotherms show typical type-I sorption isotherm with fast kinetics and good reversibility, further indicating its microporosity.

To understand better the CO_2 adsorption, we calculated the Q_{st} (isosteric heat) for 1a using the CO_2 adsorption data, which were recorded at 273 and 298 K using the virial coefficient method. As depicted in **Figure 4C**, the Q_{st} value reached 25.5 kJ mol^{-1} at zero loading, showing the good interactions of framewok–CO_2 in compound **1**, which can be ascribed to the uncoordinated O sites, N-donor of the H_3L, and the unique microporous channels. The dual-site Langmuir-Freundlich (DSLF) model was also utilized to fit the absolute adsorption isotherms of CO_2 from molecular simulations (**Figure 4D**). The result shows that the simulated CO_2 adsorption isotherms are in accordance with the experimental datas.

Magnetic Properties

Compound **1** was subjected to magnetic susceptibility measurements in the range 2–300 K at 1,000 Oe field, plots of the variable temperature magnetic susceptibility for compound **1** in the form of $\chi_m T$ vs T are presented in **Figure 5**. Compound **1** showed a higher $\chi_m T$ of about 17.17 emuK·mol^{-1} for a Co_3 unit at 300 K than the calculated spin-only value for three isolated Co^{2+} ions (5.75 emuK mol^{-1} and S = 3/2), and lies well in the range identified for octahedral Co^{2+} ions in the $^4T_{2g}$ state, which is due to the significant contribution of orbitals belonging to Co^{2+} ion in the octahedral surroundings. Upon cooling, the $\chi_m T$ value decreases sharply until the temperature descends to 11 K, then it starts to increase rapidly, attaining a minimum value of 6.84 emuK·mol^{-1} at 2 K. The behavior is consistent with antiferromagnetic phenomenon between 11–300 K. The magnetic susceptibility fits the Curie–Weiss law well above 130 K, giving C = 20.95 emuK·mol^{-1} and θ = −185.5 K,

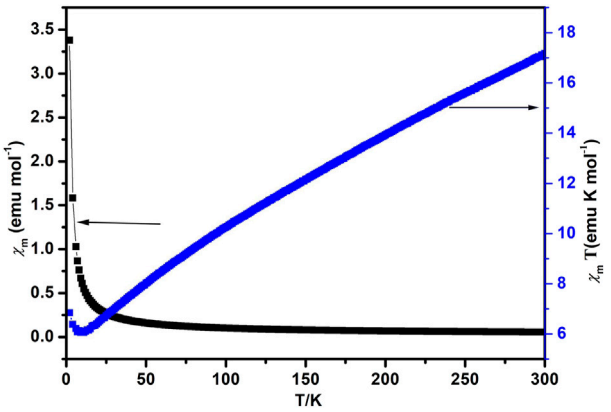

FIGURE 5 | Magnetic susceptibility of compound **1** plotted as χ_m vs. T (black) and χ_mT vs. T curves (blue).

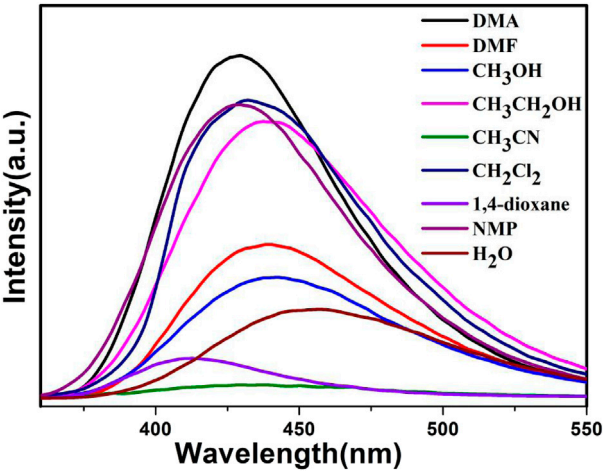

FIGURE 6 | Fluorescent spectra of compound **1a** in different solvents.

indicating an antiferromagnetic interaction between the Co_3 units.

Luminescent Emission

The solid-state emission spectra of compound **1** and H_3L ligand are depicted in **Supplementary Figure S3**. The free ligand H_3L displayed emission at 448 nm when it is excited at 330 nm. Meanwhile, compound **1** showed an emission peak at 420 nm under excitation at 345 nm, there is a blue shift of 28 nm in comparison with the H_3L ligand. The fluorescence emission of compound **1** can be associated with the corresponding intraligand transitions ($\pi^* \rightarrow \pi$ and $\pi^* \rightarrow n$) (Zhang et al., 2018).

We select compound **1a** as a representative example to study its sensing sensitivity. Dispersions of compound **1a** (3 mg) in different solvents, namely DMA, DMF, methanol, ethanol, acetonitrile, dichloromethane, 1,4-dioxane, NMP (*N*-methyl-2-pyrrolidone), and H_2O (3 ml) were prepared, and the emission spectra were measured. As shown in **Figure 6**, the luminescence intensity was affected by the solvent, especially for DMA.

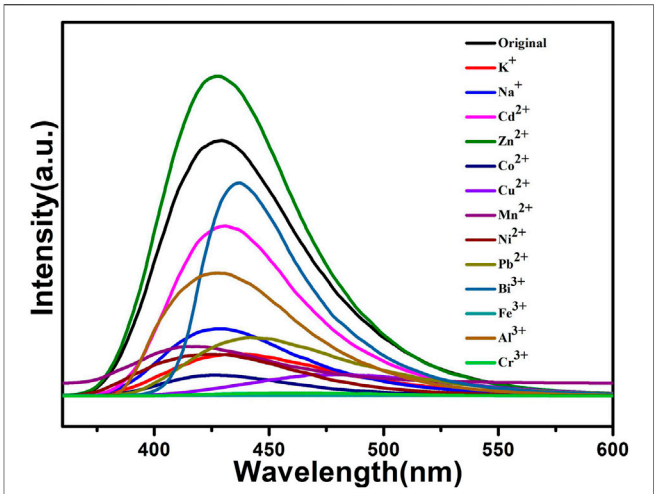

FIGURE 7 | Fluorescent analysis of 1a toward various metal ions (10^{-2} M) in DMA solution.

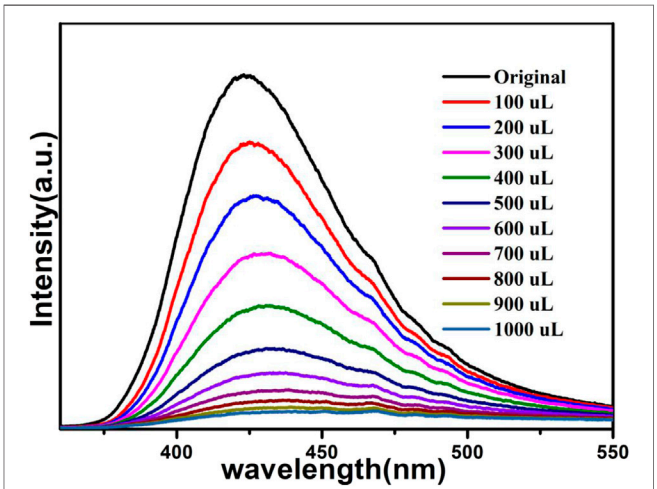

FIGURE 8 | Fluorescence of 1a in DMA containing different volumes of Fe^{3+} (1×10^{-3} M).

The above fluorescence performance prompted us to explore their potential sensing of metal ions. Samples of grounded 1a were dispersed in $M(NO_3)_x$ DMA solution separately (3 mg each sample in 3 ml, 0.01 M, $M(NO_3)_x$) (M = K^+, Cd^{2+}, Na^+, Zn^{2+}, Co^{2+}, Cu^{2+}, Mn^{2+}, Ni^{2+}, Pb^{2+}, Bi^{3+}, Fe^{3+}, Al^{3+}, Cr^{3+}), followed by ultrasonication for 1 h to obtain the uniform suspensions, the luminescence intensities of the suspensions were measured. The different emission peaks are shown in **Figure 7**, the metal ions exhibited different influence on the luminescence intensity, and the result showed that Fe^{3+} and Cr^{3+} exhibited a remarkable effect to quench the luminescence of **1a,** which indicate the high sensitivity performance of 1a towards Fe^{3+} and Cr^{3+}, the PXRD of compound 1a were measured after sensing the metal ions which remained their structural integrity (**Supplementary**

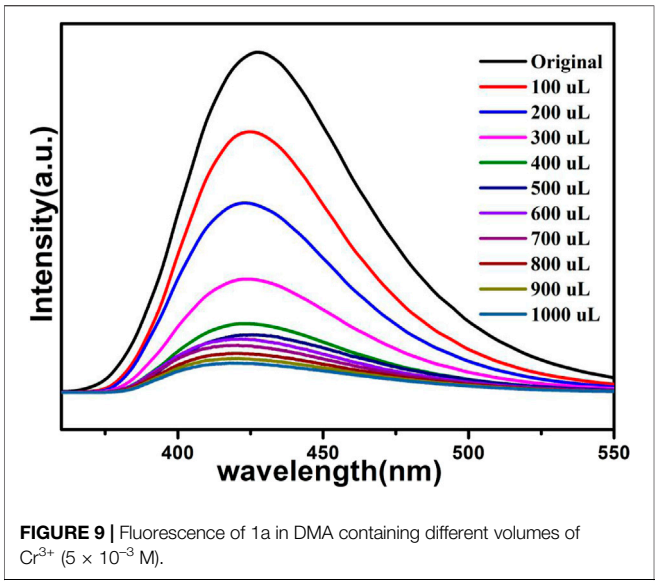

FIGURE 9 | Fluorescence of 1a in DMA containing different volumes of Cr^{3+} (5×10^{-3} M).

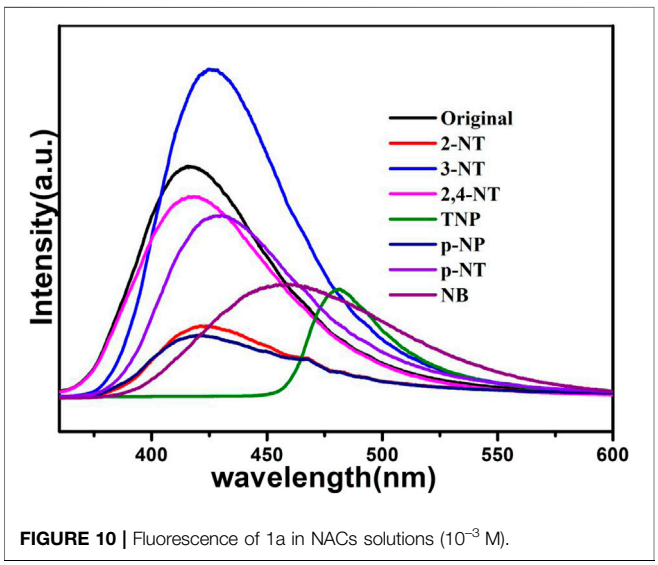

FIGURE 10 | Fluorescence of 1a in NACs solutions (10^{-3} M).

Figure S12). Furthermore, the anti-interference experiments were performed and the results indicated that the presence of other metal ions would not disturb the selective sensing of Fe^{3+} or Cr^{3+} (**Supplementary Figure S7**). Meanwhile, 3 mg samples of 1a were ground and immersed in DMA solution, sonicated for 1 h, the well-dispersed original suspensions were obtained, the Fe^{3+} or Cr^{3+} have been prepared in 1×10^{-3} M or 5×10^{-3} M DMA solution. The emission intensity decreased by gradually increasing the volume of Fe^{3+} and Cr^{3+} (**Figures 8**, **9**). Compound 1a was centrifuged and washed by DMA solvent after sensing Fe^{3+} or Cr^{3+}, the framework of the regenerated samples retained their stability, and reused for three cycles, the PXRD pattern of compound 1a is consistent with the recovered samples after three cycles (**Supplementary Figure S13**).

The fluorescence quenching efficiency can be discussed though the linear Stern–Volmer (S–V) equation: $I_0/I = 1 + K_{sv}$ [M], where I_0 and I are the fluorescence intensities before and after the addition of Fe^{3+} or Cr^{3+}, K_{sv} and [M] are the quenching constant and the concentration of Fe^{3+} or Cr^{3+}, the Stern–Volmer analysis of quenching effect on Fe^{3+} and Cr^{3+} ions show that the values of K_{sv} for Fe^{3+} and Cr^{3+} ions are $5.4 \times 10^4\ M^{-1}$, $7.83 \times 10^3\ M^{-1}$, and the limit detection of Fe^{3+} and Cr^{3+} are 0.278 mM, 1.91 mM respectively (Figs. S4 and S5).

TABLE 1 | Inhibition zone diameters of compound **1** (A), H_3L (B) and 2,2′-bipy (C).

Diameters	A	B	C
Samples of inhibition zone (mm)			
Escherichia coli	5	0	0
Staphylococcus aureus	0	0	0

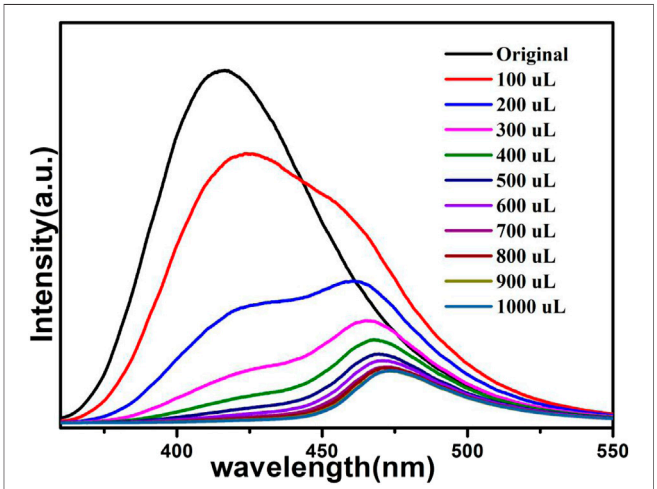

FIGURE 11 | Fluorescence of 1a in DMA containing different volumes of TNP (10^{-3} M).

The results indicate that compound 1a has the potential to act as a luminescence sensor toward Fe^{3+}, Cr^{3+}.

The NACs are explosive and environmentally deleterious. They have been used a lot in the chemical industry, so it is necessary to develop effective and quick detection of NACs. As presented in **Figure 10**, the luminescent intensity of 1a is completely quenched at 425 nm in the presence of TNP, while no obvious luminescent changes of 1a can be observed in other NACs, confirming that TNP has a pronounced emission quenching of compound **1a**, while other NACs showed less pronounced quenching.

To investigate further the sensitivity of 1a for TNP, a fluorescence titration study of TNP was conducted (**Figure 11**), the results showed that with increased incorporation of TNP solution (10^{-3} M), the luminescent intensity drastically decreased. Moreover, For the emission band of 1a, there is a large bathochromic shift of 39 nm, which is due to the energy transfer between TNP and compound **1a** (Gogia and Mandal, 2019). The quenching

effect of TNP on compound **1** can also be explained by the Stern-Volmer equation, and the details are provided in the SI. The S–V plot shows that the concentration of TNP and I_0/I possess a direct relationship over the added TNP volume range (100–1000 μL), with a linear fit coefficient value of 0.982. It is commendable that the K_{sv} value of sensing TNP reaches $3.99 \times 10^5\ M^{-1}$ (**Supplementary Figure S6**), which is one of the highest reported values for TNP sensing, and the limit detection of TNP is 0.0376 mM (Hong et al., 2017; Hua et al., 2018; Gogia and Mandal, 2019; Ghorai et al., 2019; Wang et al., 2019).

In addition, the Fe^{3+}, Cr^{3+} and TNP solutions exhibit an absorption in the 260–500 nm range, which has overlaps with the excitation of compound 1a (Figs. S8 and S9). This shows the energy of excited light is taken by Fe^{3+}, Cr^{3+} or TNP, so the transfer of energy from L^{3-} to Co^{2+} is blocked, resulting the quenching effect on compound 1a. The sensing mechanism for metal ions can be attributed to the suppression of luminescence resonance energy transfer and the enhancement of intermolecular electron transfer (Chen et al., 2018).

Antibacterial Activity

The antibacterial activities of compound **1** against *Staphylococcus aureus* and *Escherichia coli* were measured using the transparent ring method. Compound **1**, the organic linker of TCA, and 2,2′-bipy were dissolved in distilled water with a concentration of 2 mg/ml. All the cultures were incubated for 18 h at 37 °C.

The results of the inhibition zone (ZOI) are shown in **Table 1** which reveals the antibacterial potential of compound **1** against *E. Coli*, whereas compound **1** does not have antibacterial activity against *S. aureus* (**Supplemetary Figure S16**). Therefore, compound **1** has potential applications as an antibacterial agent.

CONCLUSIONS

A new fluorescent 3D supramolecular Co. coordination polymer that contains uncoordinated O atoms in the channels was synthesized and characterized. The activated 1a exhibits a strong affinity toward CO_2 molecules, with the adsorption of 74 $cm^3 \cdot g^{-1}$ (273 K, 1 atm). Magnetic measurements show that an antiferromagnetic exchange interaction exists in compound **1**. Moreover, compound 1 shows luminescence quenching with Fe^{3+}/Cr^{3+} metal ions, further studies on detection of NACs showed high performance for sensing TNP. These results may contribute to the design of more multifunctional coordiantion polymers.

DATA AVAILABILITY STATEMENT

The datasets presented in this study can be found in online repositories. The names of the repository/repositories and accession number(s) can be found below: Cambridge Crystallographic Data Centre (CCDC, https://www.ccdc.cam.ac.uk/), identification number 1961577

AUTHOR CONTRIBUTIONS

The experiments were conceived and designed by XZ; XZ, and HK. carried out the experimental work; Data were analyzed by LL, SZ, and MS; Supervision for this work was carried out by JL, and XT. All the authors contributed to the revision of manuscript.

FUNDING

This work was supported by High-tech Industrial Development Zone Science and Technology Huimin Plan of Weifang (No. 2019KJHM18), National Natural Science Foundation Youth Fund 201802104, Shandong Provincial Natural Science Foundation (No. ZR2019QB011), Project of Shandong Province Higher Educational Science and Technology Program (No. J18KA081).

SUPPLEMENTARY MATERIAL

The Supplementary Material for this article can be found online at: https://www.frontiersin.org/articles/10.3389/fchem.2021.678993/full#supplementary-material

REFERENCES

Ashraf, S., Ali, Q., Zahir, Z. A., Ashraf, S., and Asghar, H. N. (2019). Phytoremediation: Environmentally Sustainable Way for Reclamation of Heavy Metal Polluted Soils. *Ecotoxicology Environ. Saf.* 174, 714–727. doi:10.1016/j.ecoenv.2019.02.068

Cai, C., Zhao, M., Yu, Z., Rong, H., and Zhang, C. (2019). Utilization of Nanomaterials for *In-Situ* Remediation of Heavy Metal(loid) Contaminated Sediments: A Review. *Sci. Total Environ.* 662, 205–217. doi:10.1016/j.scitotenv.2019.01.180

Carter, K. P., Young, A. M., and Palmer, A. E. (2014). Fluorescent Sensors for Measuring Metal Ions in Living Systems. *Chem. Rev.* 114, 4564–4601. doi:10.1021/cr400546e

Chen, C.-H., Wang, X.-S., Li, L., Huang, Y.-B., and Cao, R. (2018). Highly Selective Sensing of Fe3+ by an Anionic Metal-Organic Framework Containing Uncoordinated Nitrogen and Carboxylate Oxygen Sites. *Dalton Trans.* 47, 3452–3458. doi:10.1039/c8dt00088c

Chen, L., Ma, N., Park, Y., Jin, S., Hwang, H., Jiang, D., et al. (2018). Highly Sensitive Determination of Iron (III) Ion Based on Phenanthroline Probe: Surface-Enhanced Raman Spectroscopy Methods. *Spectrochimica Acta A: Mol. Biomol. Spectrosc.* 197, 43–46. doi:10.1016/j.saa.2017.12.043

Chen, W.-M., Meng, X.-L., Zhuang, G.-L., Wang, Z., Kurmoo, M., Zhao, Q.-Q., et al. (2017). A superior Fluorescent Sensor for Al3+ and UO22+ Based on a Co(ii) Metal-Organic Framework with Exposed Pyrimidyl Lewis Base Sites. *J. Mater. Chem. A.* 5, 13079–13085. doi:10.1039/c7ta01546a

Chughtai, A. H., Ahmad, N., Younus, H. A., Laypkov, A., and Verpoort, F. (2015). Metal-organic Frameworks: Versatile Heterogeneous Catalysts for Efficient Catalytic Organic Transformations. *Chem. Soc. Rev.* 44, 6804–6849. doi:10.1039/c4cs00395k

Dong, C., Wu, G., Wang, Z., Ren, W., Zhang, Y., Shen, Z., et al. (2016). Selective Colorimetric Detection of Cr(III) and Cr(VI) Using Gallic Acid Capped Gold Nanoparticles. *Dalton Trans.* 45, 8347–8354. doi:10.1039/c5dt04099j

Espallargas, G. M., and Coronado, E. (2018). Magnetic Functionalities in MOFs: from the Framework to the Pore. *Chem. Soc. Rev.* 47, 533–557. doi:10.1039/C7CS00653E

Fan, J., Zhang, S., Xu, Y., Wei, N., Wan, B., Qian, L., et al. (2020). A Polyethylenimine/salicylaldehyde Modified Cellulose Schiff Base for Selective and Sensitive Fe3+ Detection. *Carbohydr. Polym.* 228, 115379. doi:10.1016/j.carbpol.2019.115379

Ghorai, P., Dey, A., Hazra, A., Dutta, A., Dutta, B., Brandão, P., et al. (2019). Cd(II) Based Coordination Polymer Series: Fascinating Structures, Efficient Semiconductors, and Promising Nitro Aromatic Sensing. *Cryst. Growth Des.*, 19, 6431–6447. doi:10.1021/acs.cgd.9b00891

Gogia, A., and Mandal, S. K. (2019). A Rational Design and green Synthesis of 3D Metal Organic Frameworks Containing a Rigid Heterocyclic Nitrogen-Rich Dicarboxylate: Structural Diversity, CO2 Sorption and Selective Sensing of 2,4,6-TNP in Water. *Dalton Trans.* 48, 2388–2398. doi:10.1039/c8dt04474k

Goswami, S., Aich, K., Das, A. K., Manna, A., and Das, S. (2013). A Naphthalimide-Quinoline Based Probe for Selective, Fluorescence Ratiometric Sensing of Trivalent Ions. *RSC Adv.* 3, 2412–2416. doi:10.1039/c2ra22624c

Guo, Z., Park, S., Yoon, J., and Shin, I. (2014). Recent Progress in the Development of Near-Infrared Fluorescent Probes for Bioimaging Applications. *Chem. Soc. Rev.* 43, 16–29. doi:10.1039/c3cs60271k

Haendel, S. R., Juan, P. H., Cristian, O. P., Cesar, A. S., and Carlos, Y. S. (2014). Antibacterial Activity against *Escherichia coli* of Cu-BTC (MOF-199) Metal-Organic Framework Immobilized onto Cellulosic Fibers. *J. Appl. Polym. Sci.* 131, 40815. doi:10.1002/app.40815

Haldar, R., Bhattacharyya, S., and Maji, T. K. (2020). Luminescent Metal-Organic Frameworks and Their Potential Applications. *J. Chem. Sci.* 132, 99. doi:10.1007/s12039-020-01797-y

Harigae, H. (2018). Iron Metabolism and Related Diseases: an Overview. *Int. J. Hematol.* 107, 5–6. doi:10.1007/s12185-017-2384-0

Hong, X.-J., Wei, Q., Cai, Y.-P., Zheng, S.-R., Yu, Y., Fan, Y.-Z., et al. (2017). 2-Fold Interpenetrating Bifunctional Cd-Metal-Organic Frameworks: Highly Selective Adsorption for CO2 and Sensitive Luminescent Sensing of Nitro Aromatic 2,4,6-Trinitrophenol. *ACS Appl. Mater. Inter.* 9, 4701–4708. doi:10.1021/acsami.6b14051

Hua, J. S., Cheng, T. T., Dong, S. J., Zhou, C. H., Huang, X. H., and Zhang, N. (2018). Multifunctional Luminescent Cd (II)-based Metal-Organic Framework Material for Highly Selective and Sensitive Sensing 2,4,6-trinitrophenol (TNP) and Fe3+ Cation. *Micropor. Mesopor. Mater.* 272, 177–183. doi:10.1016/j.micromeso.2018.06.013

Hu, Z., Deibert, B. J., and Li, j. (2014). Luminescent Metal-Organic Frameworks for Chemical Sensing and Explosive Detection. *Chem. Soc. Rev.* 43, 5815–5840. doi:10.1039/c4cs00010b

Huxford, R. C., Della Rocca, J., and Lin, W. (2010). Metal-Organic Frameworks as Potential Drug Carriers. *Curr. Opin. Chem. Biol.* 14, 262–268. doi:10.1016/j.cbpa.2009.12.012

Jia, X.-X., Yao, R.-X., Zhang, F.-Q., and Zhang, X.-M. (2017). A Fluorescent Anionic MOF with Zn4(trz)2 Chain for Highly Selective Visual Sensing of Contaminants: Cr(III) Ion and TNP. *Inorg. Chem.* 56, 2690–2696. doi:10.1021/acs.inorgchem.6b02872

Kaur, N., Tiwari, P., Kapoor, K. S., Saini, A. K., Sharma, V., and Mobin, S. M. (2020). Metal-organic Framework Based Antibiotic Release and Antimicrobial Response: an Overview. *CrystEngComm* 22, 7513–7527. doi:10.1039/d0ce01215g

Kim, D., Song, X., Yoon, J. H., and Lah, M. S. (2012). 3,6-Connected Metal-Organic Frameworks Based on Triscarboxylate as a 3-Connected Organic Node and a Linear Trinuclear Co3(COO)6 Secondary Building Unit as a 6-Connected Node. *Cryst. Growth Des.*, 12, 4186–4193. doi:10.1021/cg300686n

Kong, X.-J., Zhang, Y.-Z., He, T., Wu, X.-Q., Xu, M.-M., Wang, S.-N., et al. (2018). Two Interpenetrated Metal-Organic Frameworks with a Slim Ethynyl-Based Ligand: Designed for Selective Gas Adsorption and Structural Tuning. *CrystEngComm* 20, 6018–6025. doi:10.1039/c8ce00779a

Kurmoo, M. (2009). Magnetic Metal-Organic Frameworks. *Chem. Soc. Rev.* 38, 1353–1379. doi:10.1039/b804757j

Lan, A., Li, K., Wu, H., Olson, D. H., Emge, T. J., Ki, W., et al. (2009). A Luminescent Microporous Metal-Organic Framework for the Fast and Reversible Detection of High Explosives. *Angew. Chem. Int. Edition* 48, 2334–2338. doi:10.1002/anie.200804853

Li, B., Wen, H.-M., Zhou, W., and Chen, B. (2014). Porous Metal-Organic Frameworks for Gas Storage and Separation: what, How, and Why? *J. Phys. Chem. Lett.* 5, 3468–3479. doi:10.1021/jz501586e

Li, Y., Zhang, S., and Song, D. (2013). A Luminescent Metal-Organic Framework as a Turn-On Sensor for DMF Vapor. *Angew. Chem. Int. Ed.* 52, 710–713. doi:10.1002/anie.201207610

Liu, J., Chen, L., Cui, H., Zhang, J., Zhang, L., and Su, C.-Y. (2014). Applications of Metal-Organic Frameworks in Heterogeneous Supramolecular Catalysis. *Chem. Soc. Rev.* 43, 6011–6061. doi:10.1039/c4cs00094c

Liu, S., Yao, S., Liu, B., Sun, X., Yuan, Y., Li, G., et al. (2019). Two Ultramicroporous Metal-Organic Frameworks Assembled from Binuclear Secondary Building Units for Highly Selective CO2/N2 Separation. *Dalton Trans.* 48, 1680–1685. doi:10.1039/c8dt04424d

Lustig, W. P., Mukherjee, S., Rudd, N. D., Desai, A. V., Li, J., and Ghosh, S. K. (2017). Metal-organic Frameworks: Functional Luminescent and Photonic Materials for Sensing Applications. *Chem. Soc. Rev.* 46, 3242–3285. doi:10.1039/c6cs00930a

Ma, D., Li, B., Zhou, X., Zhou, Q., Liu, K., Zeng, G., et al. (2013). A Dual Functional MOF as a Luminescent Sensor for Quantitatively Detecting the Concentration of Nitrobenzene and Temperature. *Chem. Commun.* 49, 8964–8966. doi:10.1039/c3cc44546a

Mi, X., Sheng, D., Yu, Y. e., Wang, Y., Zhao, L., Lu, J., et al. (2019). Tunable Light Emission and Multiresponsive Luminescent Sensitivities in Aqueous Solutions of Two Series of Lanthanide Metal-Organic Frameworks Based on Structurally Related Ligands. *ACS Appl. Mater. Inter.* 11, 7914–7926. doi:10.1021/acsami.8b18320

Mishra, A., Jo, J.-H., Kim, H., Woo, S., and Chi, K.-W. (2014). A Discrete Cobalt Complex Obtained from a 1 D Coordination Polymer for Highly Selective Sensing of the Mercury(II) Ion. *ChemPlusChem* 79, 925–928. doi:10.1002/cplu.201402059

Mistri, S., Zangrando, E., Vojtíšek, P., and Manna, S. C. (2017). 1D, 2D, and 2D Parallel Interpenetrated Dicarboxylato Bridged Co(II) Metal Organic Frameworks: Synthesis, Crystal Structure, Fluorescence Sensing and Band Gap Calculation. *ChemistrySelect* 2, 2634–2642. doi:10.1002/slct.201700237

Paul, S., Manna, A., and Goswami, S. (2015). A Differentially Selective Molecular Probe for Detection of Trivalent Ions (Al3+, Cr3+and Fe3+) upon Single Excitation in Mixed Aqueous Medium. *Dalton Trans.* 44, 11805–11810. doi:10.1039/c5dt01314c

Pavlačka, M., Bajerová, P., Kortánková, K., Bláha, J., Zástěra, M., Mázl, R., et al. (2016). Analysis of Explosives Using Differential Mobility Spectrometry. *Int. J. Ion Mobil. Spec.* 19, 31–39. doi:10.1007/s12127-016-0190-7

Peng, Y. G., Zhang, Y. X., Kang, C. F., Chen, S. M., Song, L., Liu, D. H., et al. (2018). A Versatile MOF-Based Trap for Heavy Metal Ion Capture and Dispersion. *Nat. Comm.* 9, 187. doi:10.1038/s41467-017-02600-2

Rasheed, T., and Nabeel, F. (2019). Luminescent Metal-Organic Frameworks as Potential Sensory Materials for Various Environmental Toxic Agents. *Coord. Chem. Rev.* 401, 1–22. doi:10.1016/j.ccr.2019.213065

Rasheed, T., and Nabeel, F. (2019). Luminescent Metal-Organic Frameworks as Potential Sensory Materials for Various Environmental Toxic Agents. *Coord. Chem. Rev.* 401, 213065. doi:10.1016/j.ccr.2019.213065

Sadak, O., Sundramoorthy, A. K., and Gunasekaran, S. (2017). Highly Selective Colorimetric and Electrochemical Sensing of Iron (III) Using Nile Red Functionalized Graphene Film. *Biosens. Bioelectron.* 89, 430–436. doi:10.1016/j.bios.2016.04.073

Sahoo, S. K., and Crisponi, G. (2019). Recent Advances on Iron(III) Selective Fluorescent Probes with Possible Applications in Bioimaging. *Molecules* 24, 3267. doi:10.3390/molecules24183267

Saira, S., Waqas, A., Amjad, H. M., Sumaira, S., Yun, W., Yuan, Q. P., et al. (2020). Cu/$H3_BTC$ MOF as a Potential Antibacterial Therapeutic Agent against *Staphylococcus aureus* and *Escherichia coli*. *New J. Chem.* 44, 17671–17678. doi:10.1039/D0NJ04120C

Sun, C.-Y., Qin, C., Wang, X.-L., and Su, Z.-M. (2013). Metal-organic Frameworks as Potential Drug Delivery Systems. *Expert Opin. Drug Deliv.* 10, 89–101. doi:10.1517/17425247.2013.741583

Tang, Y., Chen, J., Wu, H., Yu, J., Jia, J., Xu, W., et al. (2020). A Highly Fluorescent post-modified Metal Organic Framework Probe for Selective, Reversible and Rapid Carbon Dioxide Detection. *Dyes Pigm.* 172, 107798. doi:10.1016/j.dyepig.2019.107798

Tian, C., Yin, J., Zhao, Z., Zhang, Y., and Duan, Y. (2017). Rapid Identification and Desorption Mechanisms of Nitrogen-Based Explosives by Ambient Micro-fabricated Glow Discharge Plasma Desorption/ionization (MFGDP) Mass Spectrometry. *Talanta* 167, 75–85. doi:10.1016/j.talanta.2017.02.011

VanderMeulen, H., and Sholzberg, M. (2018). Iron Deficiency and Anemia in Patients with Inherited Bleeding Disorders. *Transfus. Apher. Sci.* 57, 735–738. doi:10.1016/j.transci.2018.10.015

Wallace, K. J., Johnson, A. D. G., Jones, W. S., and Manandhar, E. (2018). Chemodosimeters and Chemoreactands for Sensing Ferric Ions. *Supramolecular Chem.* 30, 353–383. doi:10.1080/10610278.2017.1415434

Wang, J., Wu, J., Lu, L., Xu, H. J., Trivedi, M., Kumar, A., et al. (2019). A New 3D 10-Connected Cd(II) Based MOF with Mixed Ligands: A Dual Photoluminescent Sensor for Nitroaroamatics and Ferric Ion. *Front. Chem.* 7, 244. doi:10.3389/fchem.2019.00244

Wang, R., Wang, Z., Xu, Y., Dai, F., Zhang, L., and Sun, D. (2014). Porous Zirconium Metal-Organic Framework Constructed from 2D → 3D Interpenetration Based on a 3,6-Connected Kgd Net. *Inorg. Chem.* 53, 7086–7088. doi:10.1021/ic5012764

Wen, B., Shan, X. Q., and Lian, J. (2002). Separation of Cr(III) and Cr(VI) in River and Reservoir Water with 8-hydroxyquinoline Immobilized Polyacrylonitrile Fiber for Determination by Inductively Coupled Plasma Mass Spectrometry. *Talanta* 56, 681–687. doi:10.1016/s0039-9140(01)00632-4

Wollin, K. M., and Dieter, H. H. (2005). Toxicological Guidelines for Monocyclic Nitro-, Amino- and Aminonitroaromatics, Nitramines, and Nitrate Esters in Drinking Water. *Arch. Environ. Contam. Toxicol.* 49, 18–26. doi:10.1007/s00244-004-0112-2

Yamada, T., Otsubo, K., Makiura, R., and Kitagawa, H. (2013). Designer Coordination Polymers: Dimensional Crossover Architectures and Proton Conduction. *Chem. Soc. Rev.* 42, 6655–6669. doi:10.1039/c3cs60028a

Yao, C., Zhou, S., Kang, X., Zhao, Y., Yan, R., Zhang, Y., et al. (2018). A Cationic Zinc-Organic Framework with Lewis Acidic and Basic Bifunctional Sites as an Efficient Solvent-free Catalyst: CO2 Fixation and Knoevenagel Condensation Reaction. *Inorg. Chem.* 57, 11157–11164. doi:10.1021/acs.inorgchem.8b01713

Yi, F.-Y., Chen, D., Wu, M.-K., Han, L., and Jiang, H.-L. (2016). Chemical Sensors Based on Metal-Organic Frameworks. *ChemPlusChem* 81, 675–690. doi:10.1002/cplu.201600137

Yu, M.-H., Hu, T.-L., and Bu, X.-H. (2017). A Metal-Organic Framework as a "turn on" Fluorescent Sensor for Aluminum Ions. *Inorg. Chem. Front.* 4, 256–260. doi:10.1039/c6qi00362a

Zhang, J., O. Y, J., Ouyang, Y., Li, Z., Lin, Q., Chen, T., et al. (2018). Mixed-Valence Cobalt(II/III) Metal-Organic Framework for Ammonia Sensing with Naked-Eye Color Switching. *ACS Appl. Mater. Inter.* 10, 27465–27471. doi:10.1021/acsami.8b07770

Zhang, S.-R., Li, J., Du, D.-Y., Qin, J.-S., Li, S.-L., He, W.-W., et al. (2015). A Multifunctional Microporous Anionic Metal-Organic Framework for Column-Chromatographic Dye Separation and Selective Detection and Adsorption of Cr3+. *J. Mater. Chem. A.* 3, 23426–23434. doi:10.1039/c5ta07427d

Zhang, Y., Yuan, S., Day, G., Wang, X., Yang, X., and Zhou, H.-C. (2018). Luminescent Sensors Based on Metal-Organic Frameworks. *Coord. Chem. Rev.* 354, 28–45. doi:10.1016/j.ccr.2017.06.007

Zhang, Z., Yao, Z.-Z., Xiang, S., and Chen, B. (2014). Perspective of Microporous Metal-Organic Frameworks for CO2capture and Separation. *Energy Environ. Sci.* 7, 2868–2899. doi:10.1039/c4ee00143e

Zhao, X.-X., Qin, Z.-B., Li, Y.-H., and Cui, G.-H. (2018). Two Luminescent Cobalt(II) Coordination Polymers for Selective Sensing of MnO4− in Water. *Transit. Met. Chem.* 43, 597–604. doi:10.1007/s11243-018-0248-y

Zhou, E.-L., Qin, C., Tian, D., Wang, X.-L., Yang, B.-X., Huang, L., et al. (2018). A Difunctional Metal-Organic Framework with Lewis Basic Sites Demonstrating Turn-Off Sensing of Cu2+ and Sensitization of Ln3+. *J. Mater. Chem. C* 6, 7874–7879. doi:10.1039/c8tc02425a

Zhou, H.-C. J., and Kitagawa, S. (2014). Metal-Organic Frameworks (MOFs). *Chem. Soc. Rev.* 43, 5415–5418. doi:10.1039/c4cs90059f

Zhou, X. J., Guo, X. L., Liu, L. L., Shi, Z., Pang, Y., and Tai, X. S. (2019). Synthesis, Crystal Structures, and Magnetic Properties of Three Cobalt(II) Coordination Polymers Constructed from 3,5-Pyridinedicarboxylic Acid or 3,4-Pyridinedicarboxylic Acid Ligands. *Crystals* 9 (166), 1–10. doi:10.3390/cryst9030166

Conflict of Interest: The authors declare that the research was conducted in the absence of any commercial or financial relationships that could be construed as a potential conflict of interest.